*Cellular and Molecular Biology*™ **42** (8), 1181-1194
Printed in France.

0145-5680/96
1996 Cell. mol. Biol.™

# 3D RESOLVED TWO-PHOTON FLUORESCENCE MICROSCOPY OF LIVING CELLS USING A MODIFIED CONFOCAL LASER SCANNING MICROSCOPE

Karsten KÖNIG[1,✉], Ulrich SIMON[2] and Karl-Jürgen HALBHUBER[1]

[1,✉] Institute of Anatomy II, Friedrich Schiller University, D-07743 Jena, Germany
[2]Carl Zeiss Jena GmbH, Microscopy Division, D-07740 Jena, Germany

*Accepted October 4, 1996*

**Abstract** - Non-linear 3D imaging of fluorophore-labelled vital cells has been performed by femtosecond near infrared (NIR) microscopy. Ultraviolet and visible transitions of intracellular fluorophores, such as Fura-2, Calcium Green, Rhodamine 123 and fluorescent microspheres, were excited via simultaneous absorption of two 780 nm photons provided by a tunable Ti:Sapphire laser. The femtosecond laser was coupled to a conventional upright Zeiss confocal laser scanning microscope expanding its one-photon capabilities to 3D resolved two-photon microscopy. Pinhole-free non-linear 3D imaging was possible with 400 nm lateral and ≈1 µm axial resolution. Axial resolution could be further improved by using an additional detection pinhole. The NIR average power and pulse width at the sample were adjusted to be 1-4 mW and 150-200 fs, respectively. Higher power levels resulted in cell damage as demonstrated by photoinduced lysis of human erythrocytes. The powerful capabilities of this universal microscope were demonstrated by 3D imaging of two-photon excited fluorophore-labelled macrophages during phagocytosis of fluorescent microsized beads.

**Key words**: Two-photon microscopy, femtosecond microscopy, 3D imaging, vital cells

## INTRODUCTION

Three dimensional (3D) fluorescence imaging with sub-micron spatial resolution using confocal laser scanning microscopy (CLSM) has become a powerful tool in cell biology and biotechnology (e.g. Pawley, 1995). Laser sources, typically used in CLSM, are helium-neon lasers (He-Ne lasers), argon ion lasers ($Ar^+$ lasers) and argon-krypton ion lasers with discrete emission lines at 351, 364, 458, 488, 514, 543, 568, 633 and 647 nm. Using high numerical aperture (NA) objective lenses, a diffraction-limited illumination (excitation) spot in the sub-wavelength (sub-micron) range provides high lateral resolution. High axial resolution is usually achieved by using an adjustable detection pinhole in an image plane resulting in spatial supression of "out-of-focus" fluorescence ("confocal detection"). However, due to the large size of the excitation volume as compared to the detection volume, this 3D imaging technique suffers from photostress/photobleaching all along the excitation cone as well as from decreased contrast due to "out-of-focus" fluorescence (Fig. 1).

Photostress and photobleaching induced by the illumination light source turn out to be the major limitation when imaging intracellular fluorophores with electronic transitions in the ultraviolet (UV) wavelength range only, such as the endogenous fluorescent coenzymes NADH and NADPH or the exogenous fluorophores Fura-2 (calcium indicator), Indo-1 (calcium indicator) or DAPI (DNA indicator). Even UV photons with relative low

photon energy, such as UVA (320-400 nm) photons, may modify the intracellular redox state, membrane permeability and cloning efficiency. They can induce DNA breaks, giant cell production and cell death at UVA radiant exposures as low as ≈J/cm$^2$, which are accumulated during exposure times of seconds with the 365 nm line of a 50 W high-pressure mercury lamp (100 x objective) or during 10 scans with a 5 μW laser scanning beam at 351 or 364 nm and a typical 80 μs pixel dwell time (König *et al.*, 1996a). The cytotoxic UVA effects are based on non-thermal, photochemical reactions such as type I and type II photooxidation processes (charge and energy transfer) resulting in the formation of aggressive oxygen radicals and singlet oxygen, i.e. oxidative stress (Burchuladze *et al.*, 1990; Cunningham *et al.*, 1985; Foote, 1984; König *et al.*, 1996b; Tyrell and Keyse, 1990).

## PRINCIPLE OF TWO-PHOTON MICROSCOPY

Photostress and photobleaching in 3D microscopy can be significantly reduced if the excitation volume is restricted to the detection volume (Fig. 1). This can be realized by means of two-photon microscopy, where the chromophore excitation takes place only in the focal volume via the simultaneous absorption of two photons with approximately half the energy required for one-photon excitation. Thus, near infrared (NIR, 700-1200 nm) photons can excite UV and visible electronic transitions giving rise to visible fluorescence (Fig. 2). Two-

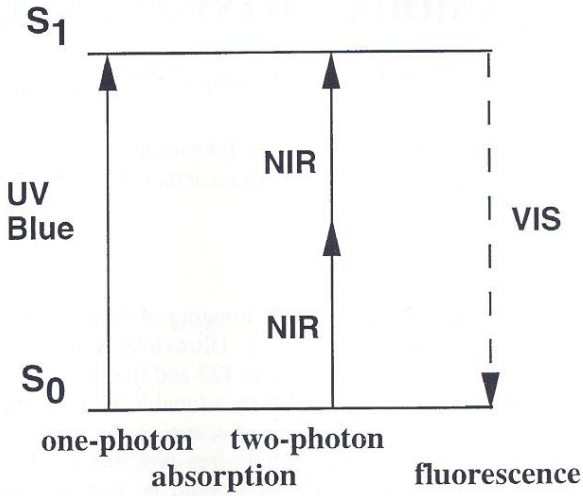


**Fig. 2** *Principle of non--resonant two-photon excitation using one NIR microbeam.* Molecules with UV and blue electronic transitions (no NIR transitions) are excited by simultaneous absorption of two NIR photons of same wavelength and can fluoresce in the visible.

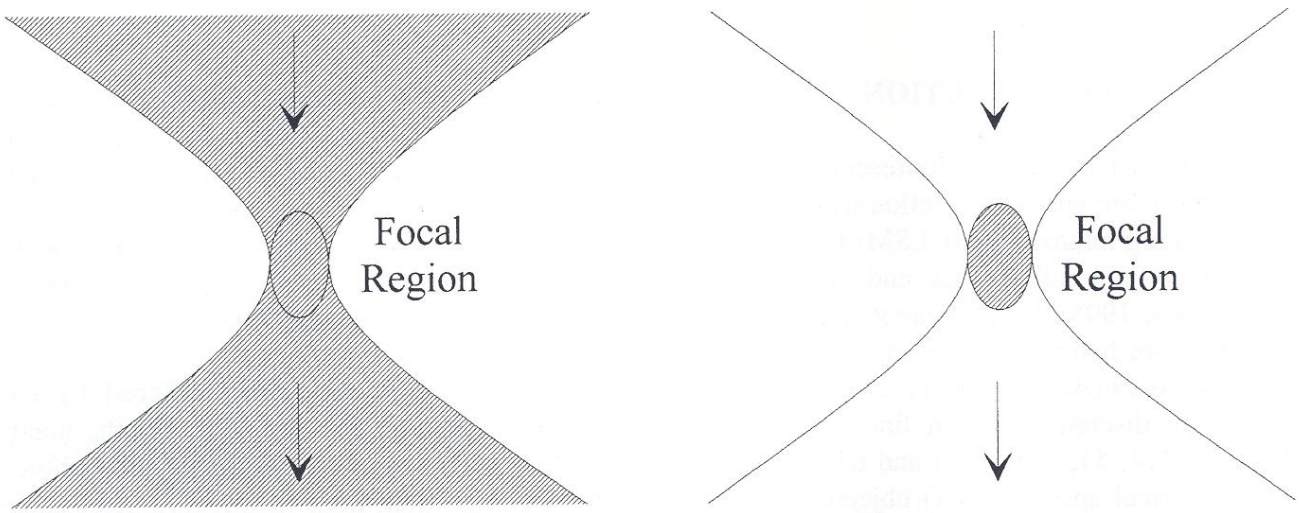


**Fig. 1** *Principle of conventional confocal fluorescence imaging* (left) *and non-linear imaging in two-photon NIR microscopes* (right). In conventional confocal microscopy, the application of pinholes in the image plane results in spatial supression of "out-of-focus" fluorescence. Because the excitation volume is larger than the detection volume, photostress and photobleaching occur through the entire depth of the cell. In contrast, the small sub-femtoliter excitation volume during two-photon excitation and the absence of efficient NIR-absorbers reduces photobleaching and stress to the focal plane.

photon excitation requires high photon concentration in time and space with typical photon flux densities on the order of $>10^{24}$ photons $cm^{-2}s^{-1}$ or $\approx MW/cm^2$ NIR intensities, respectively (Göppert-Meyer, 1931).

These high photon concentrations can be achieved by diffraction-limited focusing of continuous wave (cw) NIR laser beams with powers in the mW range (Hänninen *et al.*, 1994; König *et al.*, 1995, 1996c). In spite of the enormous intensities, cellular heating of mW-NIR-microbeams is neglible (1-2 K/100 mW; Liu *et al.*, 1995). Because of the squared dependence of the two-photon excited fluorescence on the illumination intensity and the rapid intensity decrease with the distance from the focal spot, the two-photon excitation volume in the case of high NA-objectives (NA ≥ 1) is limited to a sub-femtoliter focal region. The rate of fluorescence photons dN/dt induced by two-photon excitation can be estimated by:

$$dN/dt = \eta \cdot N \cdot \alpha \cdot \Phi^2$$

and yields $\approx 10^7$ photons $s^{-1}$ for a photon flux density of a 100 mW NIR microbeam of $\Phi \approx 10^{26}$ photons $cm^{-2}s^{-1}$, a molecule number at 15 µM concentration in the excitation volume of $N \approx 1000$, a typical two-photon absorption cross section of $\alpha = 10^{-48}$ photons $cm^4s$, and an assumed fluorescence quantum yield of 1. Considering a typical $10^{-2}$-$10^{-3}$ overall detection efficiency, image acquisition by point-scanning would require an acquisition time on the order of several min.

To realize faster image acquisition times with pixel dwell times in the microsecond range, higher excitation powers, typically on the order of hundreds of Watts, are required. However, thermal damage has to be avoided. This can be done by application of ultrashort pulses with high repetition rates and high peak power, but low average power levels in the mW range. Using such pulsed NIR microbeams the excitation photon flux densitiy is increased due to an enhanced temporal photon concentration. For well-corrected microscope optics the spatial concentration is the same as in the case of a cw microbeam (the chromatic aberration of the broadband pulses can reduce spatial photon concentration). An optimum pulse repetition rate is ≈100 MHz resulting in a 10 ns ($10^{-9}$ s) temporal separation of pulses. Because typical fluorescence lifetimes are ≤10 ns, an excited molecule can relax to the ground state before the next pulse arrives. Thus molecules can absorb two photons per pulse. Higher repetition rates result in saturation effects. In the case of pulsed microbeams with an average power level P, pulse repetition rate f, pulse width $\tau$, wavelength $\lambda$, a numerical aperture NA of the objective, the number of photon pairs non-linear absorbed per pulse and per molecule, n, can be estimated by (Denk *et al.*, 1990):

$$n \approx P^2\alpha/(\tau f^2) \cdot \pi^2 NA^4/(h^2c^2\lambda^2)$$

where h is the Planck's constant and c the speed of light.

The first two-photon microscope, realized in 1990, used a CPM-dye laser at 630 nm with 100 fs ($10^{-13}$ s) pulses (Denk *et al.*, 1990). Today's two-photon microscopes use commercially available Ti:sapphire lasers with a 300 nm tuning range from 700 - 1000 nm, pulse widths between 40 fs and 150 fs, and ≈80 MHz repetition frequency. Currently, the shortest available laser pulses are 6 fs (Fork, 1987).

The main advantages of two-photon microscopy compared to conventional "one-photon" microscopy are:

1. *Highly localized excitation.* Because two-photon excitation occurs in the focal volume only, highly localized intracellular / intramolecular micromanipulation and fluorescence excitation is possible. 3D resolved imaging does not require a "detection pinhole". Due to the inherent 3D capability, fluorescence photons can be detected with high efficiency (simplified optics, non-descanned detection possible, no spatially filtered photons).

2. *Reduced photobleaching / photodamage.* Because the NIR spectral range represents the "optical window" of cells and tissues due to the lack of efficient one-photon NIR absorbers, no photobleaching and photodamage will occur in "out-of-focus" regions.

3. *Improved signal to noise ratio.* No background fluorescence due to excitation of medium, immersion oil, contaminations or optics is present.

4. *Simplified optics.* As fluorophores with UV transitions are excited by NIR photons, two-photon microscopes do not require special UV-corrected optics. However, the development of special NIR microscope optics is desirable.

5. *Higher penetration depth.* Due to lower absorption and scattering coefficients, the NIR penetration depth in biological objects is significantely higher than for UV or visible excitation light.

6. *τ-Mapping.* The use of ultrashort exciation pulses permits the spatially-resolved detection of fluorescence lifetimes and the acquisition of fluorescence lifetime images (τ-mapping). The additional fluorescence parameter fluorescence lifetime may provide information on the microenvironment, type of bindings and number of fluorescence species (e.g. Bugiel *et al.*, 1989; Lakowicz, 1983).

These properties of two-photon microscopy makes it a suitable novel non-invasive diagnostic and micromanipulation tool in cell biology, in particular, in vital cell studies. So far, intracellular imaging of several exogenous fluorophores, such as Indo-1, Laurdan and DAPI ( Denk *et al.*, 1995; Piston *et al.*, 1994; Yu *et al.*, 1996) and endogenous fluorophores, such as NADH (Piston *et al.*, 1995; König *et al.*, 1996d), by two-photon NIR excitation has been shown. Denk *et al.* demonstrated the release of intracellular UV-labile caged compounds by two-photon excitation and to map intracellualr ion channels (Denk, 1994, Denk *et al.*, 1995). Moreover, time-resolved two-photon imaging has been realized (König *et al.*, 1996d; Piston *et al.*, 1992; So *et al.*, 1995).

In contrast to the "home-build" 2D two-photon microscopes described in the literature, we report on 3D vital cell studies using a conventional confocal laser scanning microscope equipped with a femtosecond Ti:Sapphire laser. This instrument extends its "one-photon" capabilities to 3D two-photon microscopy of living cells. The powerful capabilities of this novel microscope system are demonstrated by 3D fluorescence imaging of single fluorophore-labelled macrophages during phagocytosis of fluorescent microspheres and human erythrocytes.

## DESCRIPTION OF THE 3D CONFOCAL TWO-PHOTON FEMTOSECOND MICROSCOPE

*Experimental Set-up*

A photograph and the scheme of the experimental setup is shown in fig. 3A and 3B, respectively. A commercially available Ti:Sapphire laser (Mira Model 900-F, Coherent, Santa Clara, USA) was pumped by a 7-W-multi-line $Ar^+$ laser (Innova 310, Coherent). Tuning the short-wave cavity optics set of the Ti:Sapphire laser to its intensity maximum at 780 nm, the near-infrared laser emitted stable 130 fs-pulses at a 76 MHz repetition rate and an average power of 900 mW. An autocorrelator (APE Angewandte Physik Elektronik GmbH, Berlin, Germany) was used to monitor the pulse width of the Ti:Sapphire laser. After expanding the NIR laser beam by an 1:3-Galileian telescope, the beam was coupled into an upright confocal laser scanning microscope (LSM 310, Carl Zeiss, Jena) which was also equipped with an 543 nm-HeNe laser and an 488 nm-$Ar^+$-laser. The 80/20 neutral beam splitter of the microscope reflected 20% of the coupled laser power toward the specimen, while the remaining 80% of the laser power was absorbed in a beam stop. A pair of galvanometer scanning mirrors was used to deflect the laser beam in x- and y-direction in order to scan the

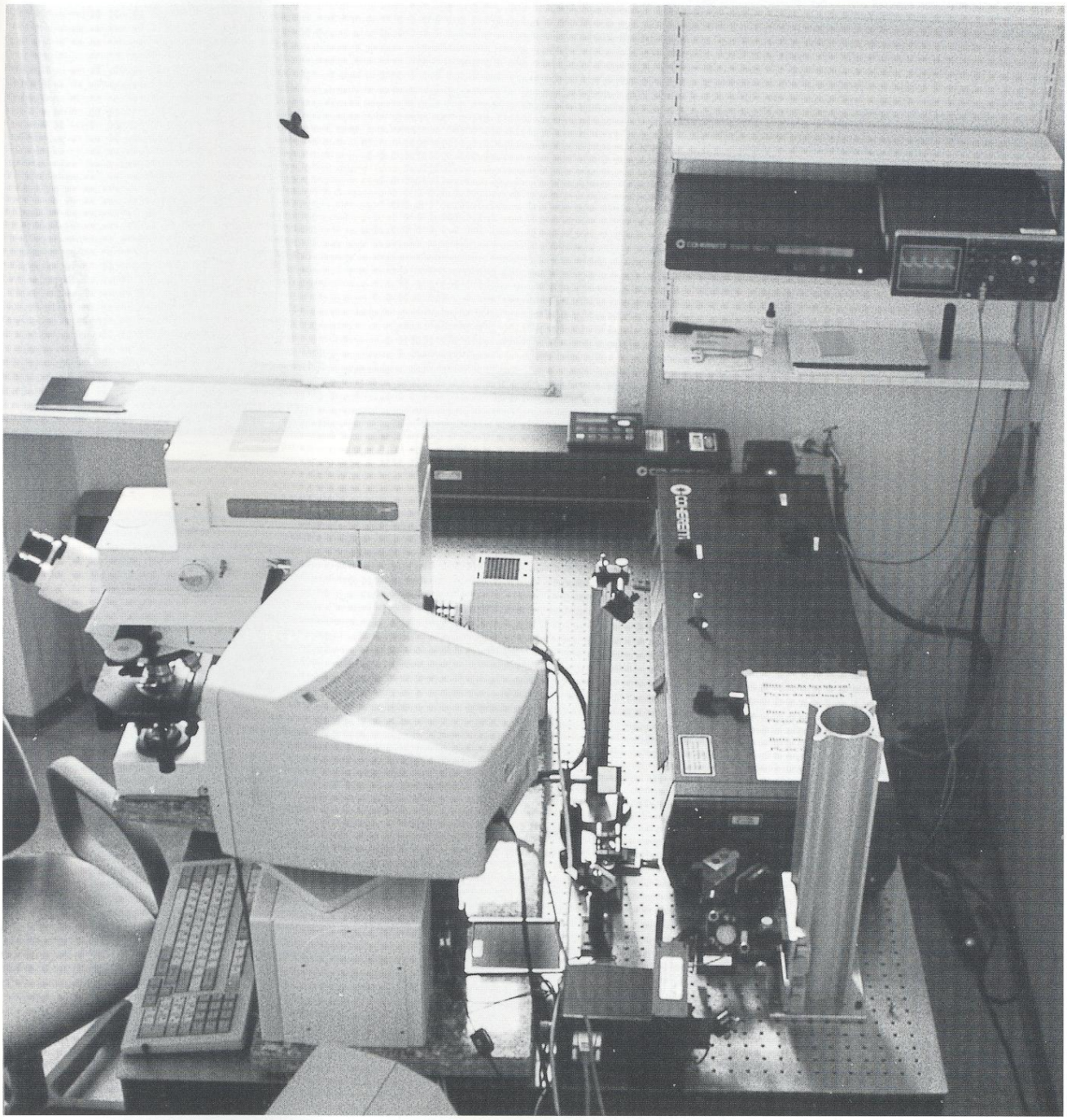

**Fig. 3** *Experimental set-up: photograph* (**A**) *and scheme* (**B**)(next page). The modified Zeiss confocal laser scanning microscope CLSM 310 expands its one-photon feasibilities to two-photon microscopy. A tunable femtosecond Ti:Sapphire laser (Mira 900, Coherent) provides the additional pulsed NIR excitation beam which is expanded by a factor 3 prior to the entrance in the microscope. The photomultipliers are equipped with 700 nm short pass filters. A beam splitter 530 was chosen for dual detection of <530 nm fluorescence and >530 nm emission, respectively.

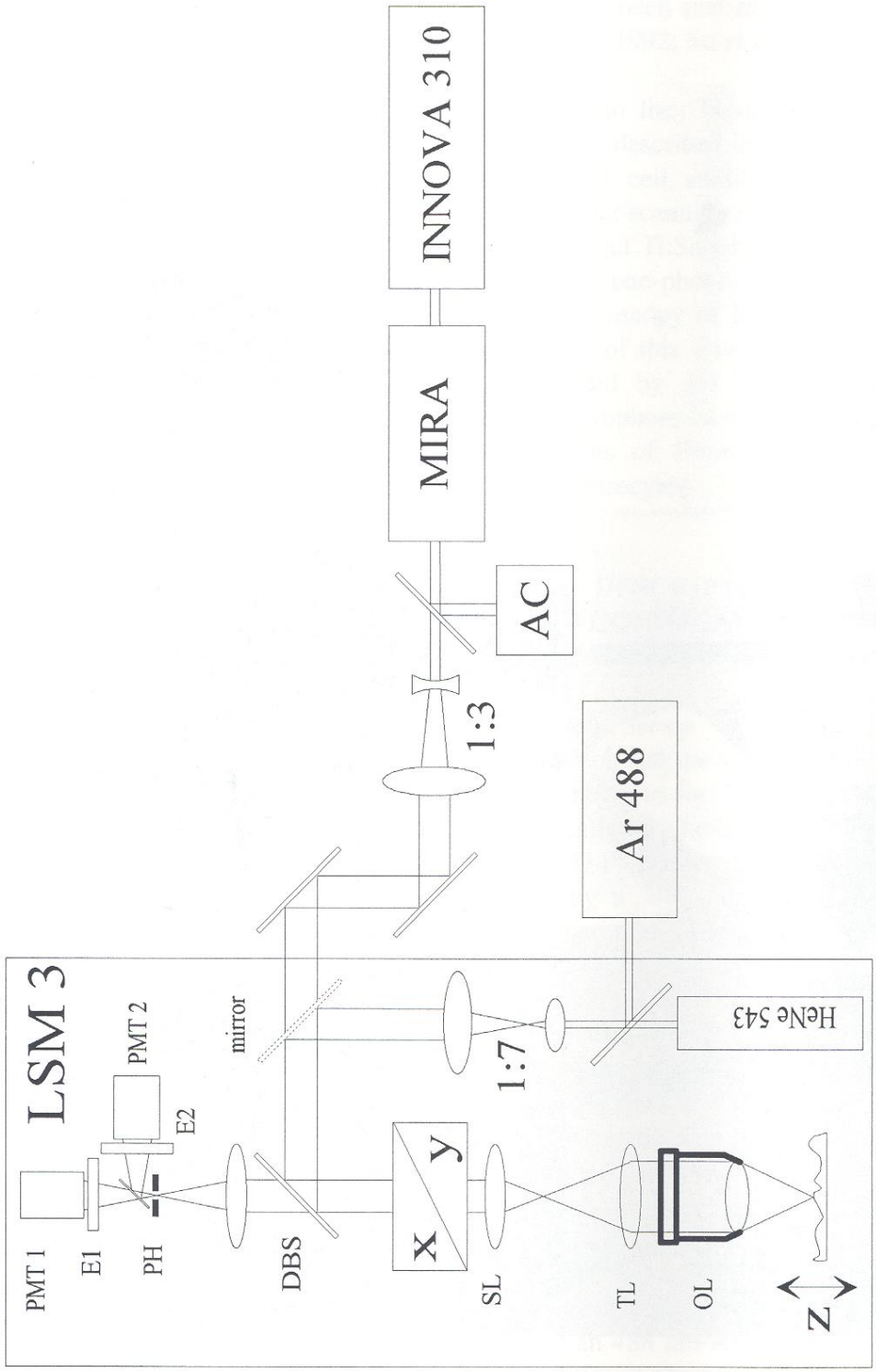


**Fig. 3B**

**Fig. 4** *Histograms of 3D fluorescence images of 100 nm beads representing point-spread-functions with full width half maxima* (FWHM) *of 0.3 µm* (lateral) *and 1.1 µm* (axial) Magn. x 63, NA= 1.25.

**Fig. 5** *Series of non-linear fluorescence images of a Fura-2 labelled macrophage during phagocytosis of fluorescent microspheres at different depths* (dz = 230 nm).

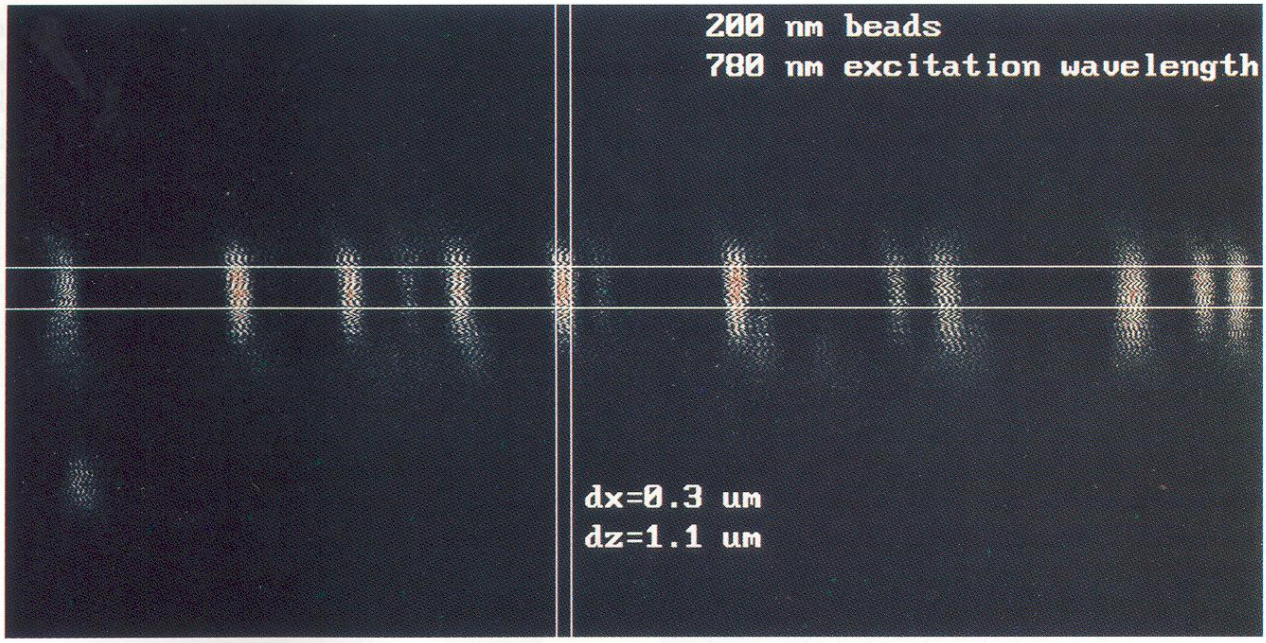
200 nm beads
780 nm excitation wavelength
dx=0.3 um
dz=1.1 um

Fig. 4

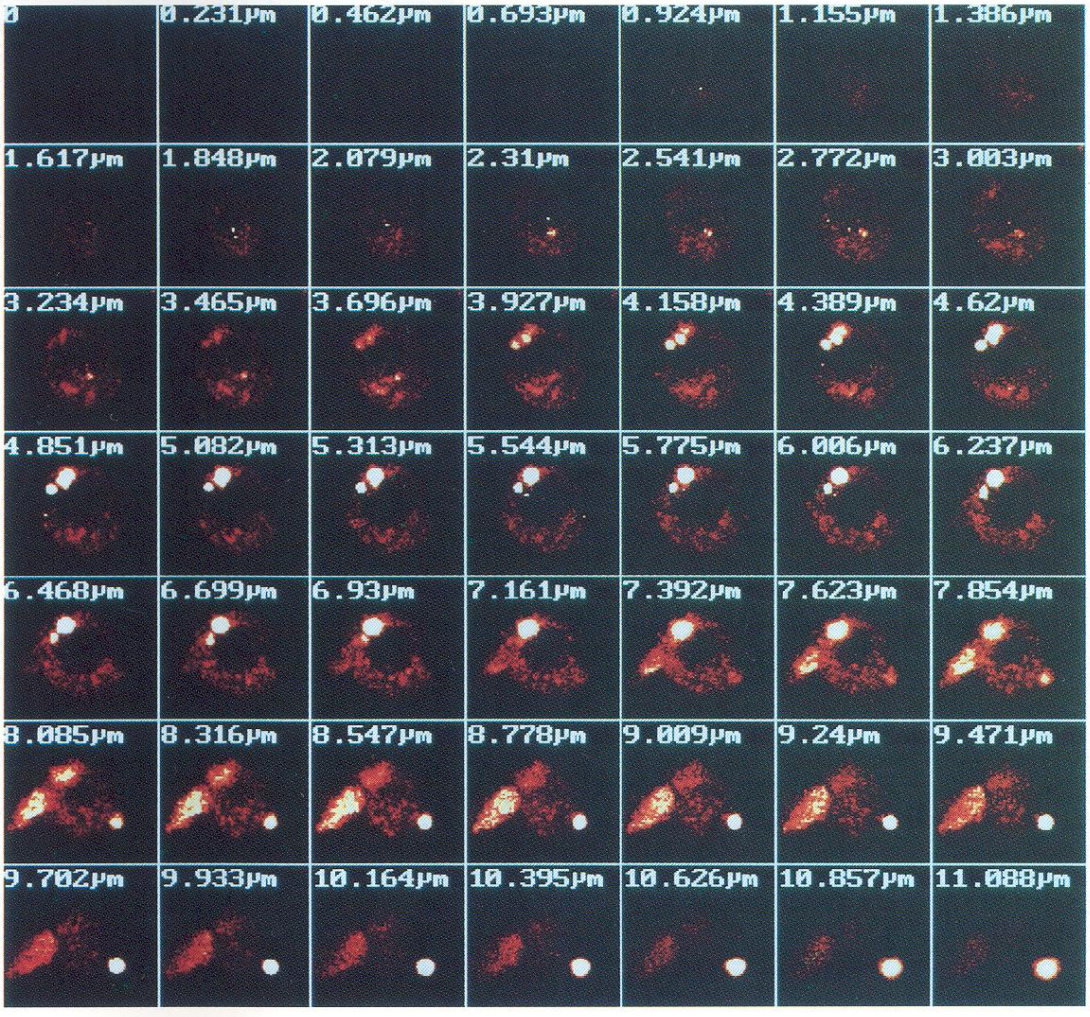
0
0.231μm
0.462μm
0.693μm
0.924μm
1.155μm
1.386μm
1.617μm
1.848μm
2.079μm
2.31μm
2.541μm
2.772μm
3.003μm
3.234μm
3.465μm
3.696μm
3.927μm
4.158μm
4.389μm
4.62μm
4.851μm
5.082μm
5.313μm
5.544μm
5.775μm
6.006μm
6.237μm
6.468μm
6.699μm
6.93μm
7.161μm
7.392μm
7.623μm
7.854μm
8.085μm
8.316μm
8.547μm
8.778μm
9.009μm
9.24μm
9.471μm
9.702μm
9.933μm
10.164μm
10.395μm
10.626μm
10.857μm
11.088μm

Fig. 5

laser point illumination accross the object field. Scan-objective lens and tube lens provided an additional magnification factor of ≈2, resulting in a near-infrared (1/e2)-laser beam diameter in the objective back focal plane (pupil) of approximately 8 mm. A high-NA objective lens (Plan-Neofluoar 63 x/1.25 oil, pupil diameter 6.5 mm) was used to focus the laser beam to an aperture-diffraction limited spot of sub-µm lateral spatial extent in the specimen. This spot acts as a point source of reflected or fluorescent light depending on the application. Throughout this work, however, only fluorescent specimens were investigated.

A cross hair slide was used in the object plane to spatially overlap the Ti:Sapphire laser beam path with the internal 543-nm-HeNe laser in the microscope. A highly reproducable mirror slider allowed to switch within 1 s between the visible lasers and the near-infrared laser, which made a systematic comparison between one-photon-visible excitation and two-photon-NIR excitation very straightforward. However, as changing the Ti:Sapphire laser wavelength (tuning the birefringent filter inside the Ti:Sapphire laser resonator) moved the beam path of the NIR laser, this superposition alignement procedure had to be repeated each time the wavelength of the femtosecond laser was changed. For the sake of simplicity, experiments described in this work have been performed at a fixed NIR excitation wavelength of 780 nm.

The overall transmittance of the optical system of the commercially available CLSM was not optimized for the NIR wavelength range and was measured to be on the order of only 8% at 780 nm from the laser entrance port to the objective pupil. This low NIR transmittance is mainly due to the use of an 80/20 neutral beam splitter instead of an optimized short pass for 780 nm. However, due to the high average power level of the Ti:Sapphire laser as much as ≈50 mW average power level at 780 nm were transmitted into the back-focal-plane of the objective lens which was shown to be more than sufficient to excite a wide variety of fluorophores.

The pulse duration of the near-infrared femtosecond laser was measured at the laser entrance port of the microscope as well as the objective back-focal-plane using the background-free non-collinear autocorrelation technique. The pulse broadening due to group velocity dispersion (GVD) in the optical system from the laser entrance port of the LSM 310 to the objective back-focal-plane (measurement without objective using the parallel beam leaving the tube lens) was found to be on the order of only 5%. The seperate measurement of the pulse broadening by the objective revealed high dispersion values on the order of ≈2000 $fs^2$ and resulted in an additional 10% broadening of input pulses. Therefore, the *in situ* pulse width was ≈150 fs. Thus, the use of a prism-sequence prechirping unit to pre-compensate for the GVD of the optical system was not required throughout this work.

The detection unit of the system consited of two PMT detection channels with one continuously variable confocal aperture for both fluorescence detection channels. To effectively prevent the scattered laser excitation radiation form reaching the detector a stack of two short pass filters with either the band edge at 600 or at 685 nm were used depending on the application. Brightfield NIR imaging (transmission mode) was performed by a third detector without short-pass filters.

*Resolution*

Depth discrimination is an intrinsic property of two-photon microscopy arising from the quadratic dependence on the excitation intensity and the strong intensity gradient in the case of high-aperture-objectives. The size of the two-photon excitation volume of our 3D two-photon microscope equipped with an 63 x PlanNeofluar oil immersion objective and its axial as well as lateral resolution, respectively, were determined by means of "pin-hole-free" 3D fluorescence imaging of fluorophore-labelled nanometer-sized microspheres (93 nm diameter, refractive index: 1.51, blue-fluorescent FluoSpheres® carboxylate-modified microspheres, Molecular Probes, USA). As seen from the

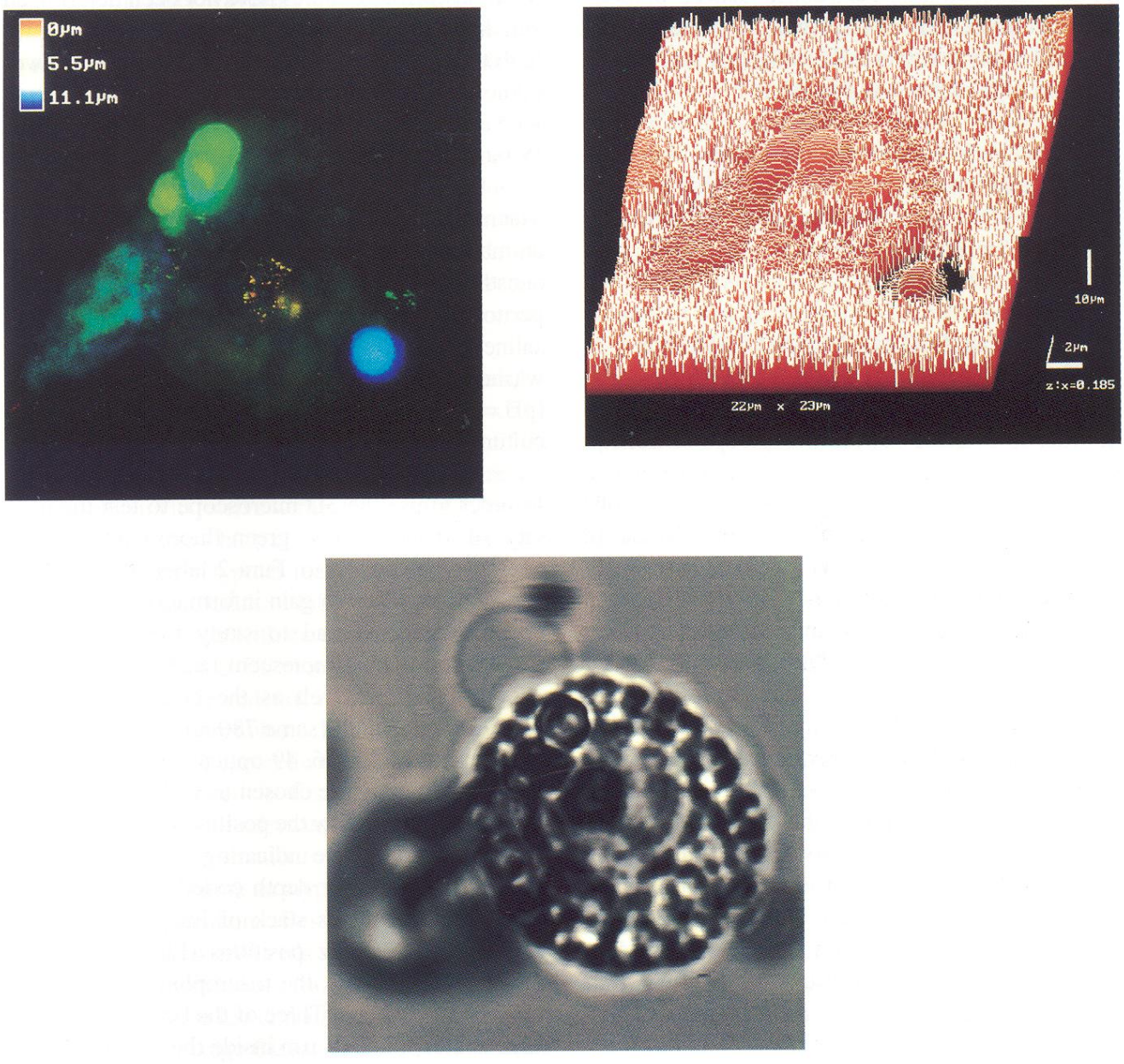


**Fig. 6** *The 3D information on the intracellular two-photon fluorescence is obtained in the false-color, depth-coded fluorescence image* (left) *and the surface topography* (right image) *which were constructed from the stack of images in fig. 6.* Transmission imaging (brightfield imaging) was performed immediately after two-photon microscopy by means of the 488 nm microbeam (lower image).

point-spread function in fig. 4, an axial and lateral resolution of 1.1 μm and 0.3 μm, respectively, were observed. Hence, 80% of the fluorescence photons originate from ≈0.1 femtoliter (0.1 $\mu m^3$) two-photon excitation volume. As a consequence, "pinhole-free" 3D fluorescence imaging of micrometer-sized samples, such as single cells, with sufficient resolution and high contrast is possible.

In the case, where higher axial resolution is demanded, the additional application of a "pinhole" in the detection plane improves the axial resolution, as shown by Stelzer *et al.* (1994).

## 3D IMAGING OF MACROPHAGES DURING PHAGOCYTOSIS

In order to evaluate our 3D microscope on cellular systems, vital rat macrophages were labelled with a number of exogenous fluorophores relevant to probe vitality, physiology and metabolism of cells and to trace single cells. In particular, the cells were incubated with the $Ca^{2+}$ indicators Fura-2 and Calcium Green or the marker of mitochondrial activity Rhodamine 123 (Molecular Probes, Eugene, USA).

At first, the intracellular accumulation of these fluorophores was probed by conventional fluorescence microscopy using either the 488 nm $Ar^+$-laser source or the 365 nm-line of the high-pressure mercury lamp as excitation radiation. In addition, the efficient 488 nm excitation of fluorescent microbeads (Fluoresbrite™ carboxy YG 2.833 ± 0.129 μm beads, excitation maximum: 458 nm, emission maximum: 540 nm, Polysciences, Warrington, USA) was demonstrated.

Following this experiment, we tried to localize these fluorophores by two-photon fluorescence imaging. All chromophores mentioned above started to fluoresce during 780 nm exposure although none of these dyes possess an one-photon absorption maximum at 780 nm/2=390 nm. The 780 nm excitation wavelength represents not the optimum two-photon excitation wavelength for all these dyes. The fluorescence intensity could be optimized by tuning the laser wavelength to the two-photon excitation maximum of the specific dye. Unfortunately, up to now the two-photon excitation spectra of most commonly used fluorophores have not been determined yet. Interestingly, the fluorescent beads showed a high two-photon fluorescence quantum yield. Two-photon excited fluorescence was detectable even with an average NIR-power as low as 0.2 mW (≈16 W pulse peak power).

Macrophages were obtained from Wistar rats. The animals were sacrificed by decapitation under ether anesthesia. Macrophages were harvested by intraperitoneal lavage with 10 ml phosphate buffered saline (PBS, 20 mM, pH = 7.4, 300 mosmol), washed in PBS and resuspended in Eagle-MEM (pH = 7.4, Gibco BRL, Eggenstein, Germany) cell culture medium incubated with the fluorophore.

In order to use the 3D microscope to test the activity of macrophages, green-fluorescent microspheres were added to Fura-2-labelled cells. 3D images were taken to gain information on the phagocytosis process and to study the intracellular localization of the fluorescent beads. Both fluorophores, Fura-2 as well as the bead fluorophore, were excited with the same 780 nm wavelength. As demonstrated in fig. 6, 49 optical sections at 2300 nm z-separation were chosen to yield 3D information. The images show the position of several beads inside the macrophage indicating successful phagocytosis. A false-color depth coded 2D image was constructed from this stack of images with color indicating different z positions (Fig. 6, left). As shown from this fig., the macrophage had dimensions of about 8 μm. Three of the beads were localized at a depth of ≈4 μm inside the cell. One bead remained at the surface outside the cell at a depth of 11 μm. In addition, image analysis allowed the construction of the surface topography of the 3D sample (Fig. 6, right). In contrast, the normal transmission image (Fig. 6, lower), taken by scanning the 488 nm microbeam, shows beads and the cell but give no information on the intracellular position and successful endocytosis, respectively.

In order to study phagocytosis of human erythrocytes, the interaction of fluorophore-labelled macrophages with the red blood cells was monitored in a first step by 488 nm-transmission imaging. By changing the laser wavelength to 780 nm, we noted laser-induced hemolysis in the transmission mode at 5 mW average power. In contrast, macrophages showed no significant cell damage as probed by PI accumulation. Reduction of the average power lead to survival of erythrocytes even during repeated scanning. To gain information on thresholds of power and radiant exposure for non--invasive two-photon imaging we studied more carefully during scanning the interaction between the femotsecond 780 nm microbeam and single erythrocytes. For that purpose we monitored changes in morphology/cytoskeleton and the onset of hemolysis during scanning. Using a frame size of 512 x 512 pixels which corresponds to an object field of 100 µm x 100 µm (63 x objective, zoom 2), we scanned single cells (up to twelve within the frame) 10 times. In order to realize a high photon density through the whole cell with a typical maximum length of 8.4 µm (Evans and Skalak, 1980) the z position was varied in 1 µm steps with each scan. We found that for a frame rate of 0.5 $s^{-1}$ the excitation beam at 2 mW *in situ* power did not induce hemolysis nor influenced cell morphology. In contrast, a reduced 0.016 $s^{-1}$ frame rate (pixel dwell time increased by a factor of 32) resulted in first changes of the cell membrane. The cell underwent a discocytic-echinocytic shape transformation with irregular spicula formation and became an atypical E2 cell according to Bessis nomenclature (Bessis, 1972). Hemolysis did not occur. At 4 mW, cells showed slight changes of membrane morphology (no hemolysis) at a 0.5 $s^{-1}$ frame rate. At the lower frame rate, cells started to "shrink" to an average 6 µm cell diameter. At 5 mW or higher, all cells underwent hemolysis at the 0.016 $s^{-1}$ frame rate.

## OUTLOOK

The unique 3D fluorescence microscope enables a novel type of 3D vital cell imaging by two-photon NIR excitation and "pinhole-free" fluorescence detection in addition to conventional confocal microscopy. Switching from one-photon VIS microscopy using the $Ar^+$ or He-Ne laser to NIR microscopy was as simple as moving the high precision mirror slider. This allowed direct comparison of NIR to visible fluorescence excitation and transmission. The use of the tunable Ti:Sapphire laser from the far red (≈ 670 nm) to ≈1000 nm provides non-linear excitation radiation of nearly all intracellular fluorophores, including chromophores with UVA transitions.

As demonstrated in this work, the use of a fixed excitation wavelength at 780 nm allows excitation of a number of commonly used intracellular fluorophores. Interestingly, the fluoresent microbeads designed for blue/green one-photon excitation appeared as two-photon fluorophor.

We found that average powers levels of the femtosecond excitation beam on the order of >5 mW at erythrocytes are sufficient to induce hemolysis. In contrast, in the case of cw 780 nm microirradiation onset of hemolysis occurred at an average power of 60 mW. Therefore, the high peak powers are responsible for cell damage. Considering a peak power of ≈300 W (5 mW average power, 150 fs, 80 MHz repetition rate) and a FWHM (full width half maximum) spot size at the focal point of ≈ 0.3 µm, the NIR intensity during the interaction of the femtosecond pulse with the cell is on the order of $GW/cm^2$. At these high intensity levels, different mechanisms may contribute to cell damage induced by femtosecond NIR microbeams. There is a high probability of non-linear cell destruction by intracellular optical breakdown (plasma formation). The cell damage would occur above certain power (intensity) thresholds. Indeed, such power dependent cell damage was found in the case of CHO cells (König *et al.*, 1996e).

Otherwise, cell damage by transient, highly localized target heating may occur. In contrast to CHO cells, erythrocytes are much better absorbers of NIR radiation. Reduced hemoglobin possess a 760

nm absorption band (molecular absorption coefficient $\alpha_{Hb}$: $\approx 1$ $mM^{-1}cm^{-1}$). Thermal-induced erythrocyte damage would have a dependence on radiant exposure as found in this study. Transient, highly localized heating could be due to high photon concentration in each submicron-illumination spot and due to the high thermal relaxation time of 8 µm cells on the order of µs compared to the 12 ns temporal pulse separation. Such heating could induce transformations in protein configuration. Considering the typical surface area of an intact human erythrocyte of 142 $\mu m^2$ (Evans and Skalak, 1980) transformation into a spherical shape without osmotic swelling would result in a cell with 6.7 µm diameter and volume increase (influx of extracellular material). In contrast, transformation in a spherical shape with no change of the typical 86 fl volume (Pschyrembel, 1994) would require a 5.5. µm diameter. We measured an average cell diameter of 6 µm at 4 mW power and 10 scans with no signs of hemoglobin efflux. The photo-induced cell damage of erythrocytes may therefore imply an isovolumetric transformation into nearly spherical cells with spicula formation, and finally hemolysis at higher radiant exposures.

The conclusion of these cell damage studies is the requirement of low average powers for non-destructive non-linear imaging using femtosecond pulses. In order to obtain sufficient fluorescence intensity, sensitive detector systems should be employed with short pass filters for high suppression of backscattered NIR excitation photons.

By designing the optics within the microscope for their application, e.g. by the use of an appropriate beam splitter, the NIR transmittance of the microscope can be significantly improved. This has the consequence, that laser output powers in the range of 20-100 mW should be sufficient for two-photon microscopy. Currently, two-photon microscopes are based on the application of large-frame, high-cost water-cooled $Ar^+$-laser pumped Ti:Sapphire lasers of high power consumption in connection with large optical tables. The laser output is typically on the order of 1 W. The operation of the equipment requires skilled laser-engineers or laser physicists. Currently the first air-cooled, compact diode-pumped solid state lasers at 532 nm are on the market as powerful $Ar^+$-laser alternatives. These lasers can be used to pump Ti:Sapphire lasers. Considering the demand of low *in situ* power and the wide range of excitable fluorophores at one NIR wavelength, e.g. 780 nm, the design of a compact, low-cost "turn-key" solid-state femtosecond NIR laser for two-photon microscopy, such as miniaturized Ti:Sapphire lasers, diode-pumped Cr:LiSAF lasers, or fiber lasers (e.g. Knopf *et al.*, 1995; Reed *et al.*, 1996) appears possible.

Besides the construction of appropriate laser sources, two other demands for efficient two-photon microscopy are: i) the design of microscopes with optimized NIR optics, including the development of special objectives with high NIR transmittance and low optical dispersion, and ii) the design of appropriate two-photon fluorescence probes in cellular and molecular biology. In a first step, the varity of well-known exogenous and endogenous cell fluorophores should be characterized to their two-photon excitation behaviour (Xu and Webb, 1996). It should be noted that two-photon excitation spectra may significantly differ from one-photon fluorescence excitation spectra with the wavelength axis doubled (e.g. Jiang, 1989; Kennedy and Lytle, 1986).

Two-photon microscopes, as potentially simple and inexpensive tools, open novel applications in cell biology, medicine and biotechnology. Besides the non-destructive "pinhole-free" 3D imaging of vital cells as an improvement to conventional fluorescence microscopy there is the chance to perform intracellular 3D micromanipulations in a sub-femtoliter two-photon excitation volume. For example, photolabile "caged" compounds (e.g. "caged" calcium) can be released in a well defined intracellular volume by femtosecond NIR microbeams (e.g. Denk *et al.*, 1995). This allows a highly localized variation of intracellular specific ion gradients. Another potential application is

multi-dye excitation with one NIR wavelength as demonstrated. This may also be useful in biotechnology for multi-gene detection by fluorescence *in situ* hybridization.

**Acknowledgments** - The authors are gratefull for the excellent support by Dr. Thieme from Coherent (Dieburg, Germany) and by Mrs. Lemke and Mrs. Eschler (Institute of Anatomy II, Jena, Germany).

## REFERENCES

Bessis, M., Red cell shapes. An illustrated classification and its rationale. *Nouv. Rev. franc. Hématol.* 1972, **12**: 721-746.

Bugiel, I., König, K. and Wabnitz, H., Investigation of cells by fluorescence laser scanning microscopy with subnanosecond time resolution. *Lasers in Life Sci.* 1989, **3(1)**: 47-53.

Burchuladze, T.G., Sideris, E.G. and Fraikin, G.I., Sensitized NADH formation of single-stranded breaks in plasmid DNA upon the action of near UV radiation. *Biofizika* 1990, **35**: 722-725.

Cunningham, M.L., Johnson, J.S., Giovanazzi, S.M. and Peak, M.J., Photosensitized production of superoxide anion by monochromatic (290-405 nm) ultraviolet irradiation of NADH and NADPH coenzymes. *Photochem. Photobiol.* 1985, **42(2)**: 125-128.

Denk, W., Two-photon scanning photochemical microscopy used to map the distribution of ligand gated ion channels. *Soc. Neurosci.* 1994, **19(1)**: 91.

Denk, W., Piston, D.W. and Webb, W.W., Two-photon molecular excitation in laser-scanning microscopy. In: *Handbook of biological Confocal Microscopy.* 2d. ed., Pawley, J.B. (ed.), Plenum Press, New York, 1995, pp. 445-458.

Denk, W., Strickler, J.H. and Webb, W.W., Two-photon laser scanning fluorescence microscope. *Science* 1990, **248**: 73-76.

Evans, E.A. and Skalak, R. (eds.), *Mechanics and Thermodynamics of Biomembranes.* CRC Press. Boca Raton, Florida, 1980.

Foote, C.S., Mechanisms of photooxygenation. In: *Porphyrin Localization and Treatment of Tumors,* Doiron, D.R. and Gomer, C.J. (eds.), Alan R. Liss, New York, 1984, pp. 3-18.

Fork, R.L., Brito Cruz, C.H., Becker, P.C. and Shank, C.V., Compression of optical pulses to six femtoseconds by using cubic phase compensation. *Opt. Lett.* 1987, **12(7)**: 483-485.

Göppert-Meyer, M., Über Elementarakte mit zwei Quantensprüngen. Göttinger Dissertation. *Ann. Phys.* 1931, **9**: 273-294.

Hänninen, P.E., Soini, E. and Hell, S.W., Continuous wave excitation two-photon fluorescence microscopy. *J. Microsc.* 1994, **176**: 222-225.

Jiang S., Two-photon spectroscopy of biomolecules. *Prog. React. Kinet.* 1989, **15**: 77-92.

Kennedy, S.M. and Lytle, F.E., P-Bis(o-methylstyryl)benzene as a power squared tensor for two-photon absorption measurements between 537 and 694 nm. *Anal. Chem.* 1986, **58**: 2643-2647.

Knopf, D., Weingarten, K.J., Brovelli, L.R., Kamp, M. and Keller, U., Diode-pumped 100fs-passively mode-locked Cr:LiSAF laser with an antiresonant Fabry-Perot saturable absorber. *Opt. Lett.* 1995, **19**: 2143-2145.

König, K., Berns, M.W. and Tromberg, B.J., Time-resolved and steady-state fluorescence measurements of NADH-alcohol dehydrogenase complex during UV-A exposure. *J. Photochem. Photobiol. B.* 1996b, in press, Accepted: March 18, 1996.

König, K., Krasieva, T., Bauer, E., Fiedler, U., Berns, M.W., Tromberg, B.J. and Greulich, K.O., Cell damage by UVA radiation of a mercury microscopy lamp probed by autofluorescence modifications, cloning assay and comet assay. *J. biomed. Optics* 1996a, **1(2)**: 217-222.

König, K., Liang, H., Berns, M.W. and Tromberg, B.J., Cell damage by near-IR microbeams. *Nature* 1995, **377**: 20-21.

König, K., Liang, H., Berns, M.W. and Tromberg, B.J., Cell damage in near infrared multimode optical traps due to multiphoton absorption. *Opt. Lett.* 1996c, **21(4)**: 1090-1092.

König, K. and Schneckenburger, H., Laser-induced autofluorescence for medical diagnosis. *J. Fluoresc.* 1994, **4**: 17-40.

König, K., So, P.T.C., Mantulin, W.W., Tromberg, B.J. and Gratton, E., Two-photon excited lifetime imaging of autofluorescence in cells during UVA and NIR photostress. *J. Microsc.* 1996d, **183**: 197-204.

König, K., So, P.T.C., Mantulin, W.W. and Gratton, E., Cellular response to near-infrared femtosecond laser pulses in two-photon microscopes. *Opt. Lett.* 1996e, in press, Accepted: October 28, 1996.

Lakowicz, J.R., *Principles of Fluorescence Spectroscopy,* Plenum Press, New York, 1983.

Liu, Y., Cheng, D., Sonek, G.J., Berns, M.W., Chapman, C.F. and Tromberg, B.J., Evidence for localized cell heating induced by infrared optical tweezers. *Biophys. J.* 1995, **68**: 2137-2144.

Pawley, J.B., *Handbook of biological confocal Microscopy.* 2d. ed., Plenum Press. New York, 1995.

Piston, D.W., Kirby, M.S., Cheng, H. and Lederer, W.J., Two-photon excitation fluorescence imaging of three-dimensional calcium-ion activity. *Appl. Optics* 1994, **33**: 662-669.

Piston, D.W., Masters, B.R. and Webb, W.W., Three-dimensionally resolved NAD(P)H cellular metabolic redox imaging of the *in situ* cornea with two-photon excitation laser scanning microscopy. *J. Microsc.* 1995, **178(1)**: 20-27.

Piston, D.W., Sandison, D.R. and Webb, W.W., Time resolved fluorescence imaging and background rejection by two-photon excitation in laser scanning microscopy.

*Proc. SPIE.* 1992, **1640**: 379-389.

Pschyrembel. *Klinisches Wörterbuch.* Walter de Gruyter. Berlin, 1994.

Reed, M.K., Steiner-Shepard, M.K. and Negus, D.K., An efficient diode-based Ti:sapphire laser. Paper WE2. In: *Proceedings: Advanced solid State Lasers.* San Fransisco, 1996.

So, P.T.C., French, T., Yu, W.M., Berland, K.M., Dong, C.Y. and Gratton, E., Time-resolved fluorescence microscopy using two-photon excitation. *Bioimaging* 1995, **3**: 1-15.

Stelzer, E.H.K., Hell, S., Lindek, S., Stricker, R., Pick, R., Storz, C., Ritter, G. and Salmon, N., Non-linear absorption extends confocal fluorescence microscopy into the ultra-violet regime and confines the illumination volume. *Opt. Commun.* 1994, **104**: 223-228.

Tyrell, R.M. and Keyse, S.M., The interaction of UVA radiation with cultured cells. *J. Photochem. Photobiol.* 1990, **4**: 349-361.

Xu, C. and Webb, W.W., Measurement of two-photon cross sections. *J. opt. Soc. Am. B.* 1996, **13(3)**: 481-491.

Yu, W., So, P.T.C., French, T. and Gratton, E., Fluorescence generalized polarization of cell membranes: a two-photon scanning microscopy approach. *Biophys. J.* 1996, **70**: 626-636.